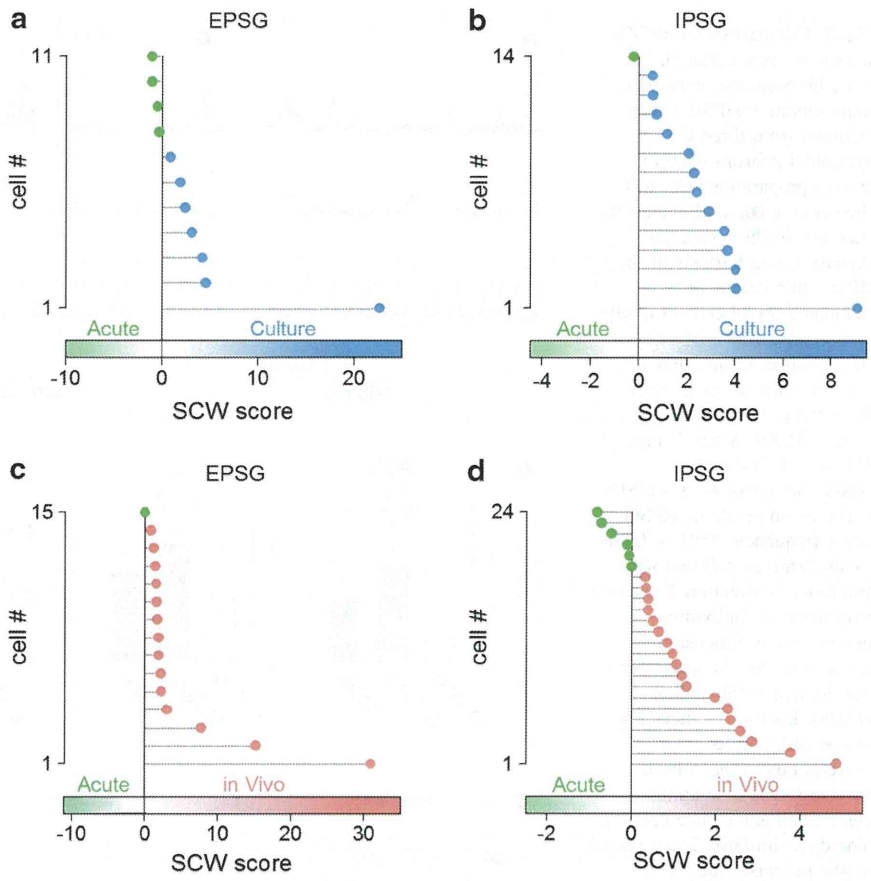

Fig. 4 SCW judged the majority of slice culture data sets as in vivo-like. **a** The *abscissa* indicates SCW scores, with higher values representing that the EPSG parameters of a given data set are more similar to those obtained from slice cultures. The ordinate indicates individual cells. The order of 11 in vivo cells was sorted along their SCW scores. SCWs judged EPSGs of 7 of the 11 in vivo cells (64 %) as slice culture-like. **b** Same as **a**, except for IPSGs. SCWs judged IPSGs in 13 of 14 in vivo cells (93 %) as slice culture-like. **c** The *abscissa* indicates SCW scores, with higher values representing that the EPSG parameters of a given data set are more similar to those obtained from in vivo recordings. The ordinate indicates individual cells. The order of the 15 cells in slice cultures was sorted along their SCW scores. SCWs judged 14 of 15 cells (93 %) as in vivo-like. **d** Same as **c**, except for IPSGs in vivo. SCWs judged IPSGs in 18 of 24 cells (75 %) as in vivo-like

the parameters of synaptic activity without any human bias, because SCW can estimate the features of skewness and kurtosis in each cell even when the parameters are largely distributed.

For sEPSGs and sIPSGs, SCW was exposed sequentially to individual data sets of slice cultures and acute slices, which consisted of the CV, skewness, kurtosis of PSGs, and the PSGs event frequency. Based on these parameters, SCW gradually calculated a weight vector during this learning phase and thereby learned the overall parameter tendencies of slice cultures and acute slices. We defined the dot product of the weight vector and data set parameters as the SCW score; a more positive SCW score indicates a higher similarity to slice cultures. After the learning phase, we obtained the SCW score of each in vivo data set by inputting its parameters to the trained SCW (test phase). In other words, the trained SCW was asked to judge whether a given in vivo data set is more "slice culture-like" or "acute slice-like" based on its prior knowledge about the parameter tendencies of slice cultures and acute slices.

For the sEPSG data sets of in vivo preparations, SCWs gave positive SCW scores in 7 of the 11 in vivo cells (64 %), that is, more than a half of the in vivo cells were judged to be more similar to slice-cultured cells rather than acute-slice cells (Fig. 4a). For the sIPSG data sets, SCWs concluded that 13 of 14 cells (93 %) were more similar to slice-cultured cells (Fig. 4b). These results suggest that in vivo preparations and slice cultures are similar in both EPSGs and IPSGs.

To further confirm this tendency, we next trained the SCW machine using the data sets of in vivo preparations and acute slices (learning phase) and asked it whether individual data sets of slice cultures are more similar to those in the parameters of in vivo preparations or acute slices (test phase). For the sEPSG data sets of slice cultures, SCWs judged 14 of 15 cells (93 %) as in vivo cell-like rather than acute-slice cell-like (Fig. 4c). For the sIPSG data sets, SCWs concluded that 18 of 24 cells (75 %) were more similar to in vivo cells (Fig. 4d).

Discussion

In this work, we compared spontaneous activity of hippocampal neurons among acute slices, cultured slices, and in vivo networks and found that, as a whole, spontaneous

activity of slice cultures was more similar to that of in vivo preparations in terms of both spike outputs and synaptic inputs. Therefore, cultured slices are suggested to be a useful tool for investigating spontaneous network activity.

We used mice for in vivo preparations and acute slices, whereas we used rats for slice cultures. This is simply due to the routine experimental systems of our laboratory. We do not think that different species affected our results, because the spontaneous activity level in the hippocampus is almost equivalent between rats and mice; the mean firing rate of rat hippocampal neurons is reported to be about 0.27 Hz during quiet awake states [26] and does not differ from the in vivo firing rate in our head-restricted mouse (0.14 ± 0.21 Hz). One of the remarkable differences between in vivo and in vitro preparations is that in vivo animals drift across different brain states, including actively exploring, resting, and sleeping states. The firing rates of neurons and the oscillation powers of local field potentials change depending on these behavioral states [3, 26]. We fixed the head of the mice to a stereotaxic frame; thus, we expected that the mice spent the majority of their time for quite awake or sleep. However, we cannot strictly determine which in vivo state corresponded to the spontaneous state of our in vitro preparations. Nonetheless, it is notable that in vivo data were still similar to cultured slice data even when all in vivo data were blindly pooled irrespective of their states. On the other hand, we leave open the question of whether some aspect in the activity of acute slices may represent a specific state of in vivo animals more faithfully.

The mean firing rates are thought to represent an aspect of information coding [9, 31, 37]. The similarity of the mean firing rates between in vivo preparations and slice cultures suggest that these preparations share a common circuit basis for spontaneous spiking. During cultivation, slice cultures restore the complexity of their neuronal network through neuritogenesis and synaptogenesis. This self-organization process occurs spontaneously depending on the intrinsic network formation rules; note that slice cultures do not receive sensory inputs and thus mature purely through their own activity and the inherent laws. Our data indicate that such spontaneously emerging networks can behave like in vivo networks. Thus, cultivation ameliorates artificially damaged networks in acute slices. This idea is consistent with a previous report showing that the difference of evoked unitary synaptic activity in monosynaptically connected neuron pairs between cultured and acute hippocampus slices depends on the density of synaptic connections [5]; the CA3-CA1 excitatory connection probability is 76 % in slice cultures and 6 % in acute slices, and the CA3-CA3 connection probability is 56 % in slice cultures and 1.5 % in acute slices. However, these data must be interpreted with caution, because the circuit density is subject to developmental changes during cultivation. Indeed, the amplitudes of evoked EPSPs are known to change as a function of days in vitro [12, 23]. In the present work, we used slice cultures after 6–12 days in vitro. Evaluations using electrophysiology and morphology demonstrate that the developmental maturation of hippocampal neurons under cultured conditions is almost equivalent to day-matched neurons in vivo [4]. Based on this calculation, our slice cultures are estimated to correspond to the neural conditions in 13-to-19-day-old mice. In general, cortical neurons generate widely synchronized activity during early development [24], and the activity patterns become more decorrelated in the course of neuronal network maturation [10, 32]. After that, the firing rates are kept almost constant over long postnatal days [20]. We believe that all our preparations already reached the final stage of maturation, because their spiking activity was rather sparse.

The high-order sEPSG kinetics parameters, such as CV, skewness, and kurtosis, reflect neuronal synchronization. Synchronized synaptic inputs come from the population activity of presynaptic cell ensembles and cause large membrane potential fluctuations [8, 40]. The fact that these parameters were similar between in vivo preparations and slice cultures suggests that the entire network activity patterns are also organized in a similar manner. On the other hand, the sIPSG parameters were not necessarily similar between in vivo preparations and slice cultures and did not differentiate in the MDS space. A possible explanation is that the axons of GABAergic interneurons are more spared after slicing relative to those of pyramidal cells [38], because hippocampal GABAergic neurons tend to innervate nearby neurons [11]. Therefore, compared to excitatory synaptic activity, spontaneous inhibitory activity may not be severely reduced in acute slices. However, SCW separated IPSGs in acute slices from those of in vivo parameters and slice cultures. Given that firings of inhibitory neurons are driven by excitatory inputs, we believe spontaneous inhibitory activity is also affected in acute slices even though their network per se is relatively intact.

Acknowledgments We are grateful to Dr. Hiroshi Ban (CiNET) for his technical support for soft confidence weighted. This work was supported by Kakenhi (22115003; 26250003; 25119004).

Conflict of interest The authors declare no competing financial interests.

References

1. Arieli A, Sterkin A, Grinvald A, Aertsen A (1996) Dynamics of ongoing activity: explanation of the large variability in evoked cortical responses. Science 273:1868–1871
2. Beggs JM, Plenz D (2003) Neuronal avalanches in neocortical circuits. J Neurosci 23:11167–11177

3. Buzsaki G, Leung LW, Vanderwolf CH (1983) Cellular bases of hippocampal EEG in the behaving rat. Brain Res 287:139–171
4. De Simoni A, Griesinger CB, Edwards FA (2003) Development of rat CA1 neurones in acute versus organotypic slices: role of experience in synaptic morphology and activity. J Physiol 550:135–147
5. Debanne D, Guerineau NC, Gahwiler BH, Thompson SM (1995) Physiology and pharmacology of unitary synaptic connections between pairs of cells in areas CA3 and CA1 of rat hippocampal slice cultures. J Neurophysiol 73:1282–1294
6. Fiser J, Chiu C, Weliky M (2004) Small modulation of ongoing cortical dynamics by sensory input during natural vision. Nature 431:573–578
7. Gahwiler BH, Capogna M, Debanne D, McKinney RA, Thompson SM (1997) Organotypic slice cultures: a technique has come of age. Trends Neurosci 20:471–477
8. Gasparini S, Magee JC (2006) State-dependent dendritic computation in hippocampal CA1 pyramidal neurons. J Neurosci 26:2088–2100
9. Geisler WS, Albrecht DG, Salvi RJ, Saunders SS (1991) Discrimination performance of single neurons: rate and temporal-pattern information. J Neurophysiol 66:334–362
10. Golshani P, Goncalves JT, Khoshkhoo S, Mostany R, Smirnakis S, Portera-Cailliau C (2009) Internally mediated developmental desynchronization of neocortical network activity. J Neurosci 29:10890–10899
11. Gulyas AI, Miles R, Hajos N, Freund TF (1993) Precision and variability in postsynaptic target selection of inhibitory cells in the hippocampal CA3 region. Eur J Neurosci 5:1729–1751
12. Ikegaya Y (1999) Abnormal targeting of developing hippocampal mossy fibers after epileptiform activities via L-type Ca2+ channel activation in vitro. J Neurosci 19:802–812
13. Ikegaya Y, Le Bon-Jego M, Yuste R (2005) Large-scale imaging of cortical network activity with calcium indicators. Neurosci Res 52:132–138
14. Ikegaya Y, Aaron G, Cossart R, Aronov D, Lampl I, Ferster D, Yuste R (2004) Synfire chains and cortical songs: temporal modules of cortical activity. Science 304:559–564
15. Ikegaya Y, Sasaki T, Ishikawa D, Honma N, Tao K, Takahashi N, Minamisawa G, Ujita S, Matsuki N (2012) Interpyramid spike transmission stabilizes the sparseness of recurrent network activity. Cereb Cortex.
16. Ishikawa D, Matsumoto N, Sakaguchi T, Matsuki N, Ikegaya Y (2014) Operant conditioning of synaptic and spiking activity patterns in single hippocampal neurons. J Neurosci 34:5044–5053
17. Kandel ER, Spencer WA (1961) Electrophysiology of hippocampal neurons. II. After-potentials and repetitive firing. J Neurophysiol 24:243–259
18. Kenet T, Bibitchkov D, Tsodyks M, Grinvald A, Arieli A (2003) Spontaneously emerging cortical representations of visual attributes. Nature 425:954–956
19. Koyama R, Muramatsu R, Sasaki T, Kimura R, Ueyama C, Tamura M, Tamura N, Ichikawa J, Takahashi N, Usami A, Yamada MK, Matsuki N, Ikegaya Y (2007) A low-cost method for brain slice cultures. J Pharmacol Sci 104:191–194
20. Langston RF, Ainge JA, Couey JJ, Canto CB, Bjerknes TL, Witter MP, Moser EI, Moser MB (2010) Development of the spatial representation system in the rat. Science 328:1576–1580
21. Mao BQ, Hamzei-Sichani F, Aronov D, Froemke RC, Yuste R (2001) Dynamics of spontaneous activity in neocortical slices. Neuron 32:883–898
22. Mizunuma M, Norimoto H, Tao K, Egawa T, Hanaoka K, Sakaguchi T, Hioki H, Kaneko T, Yamaguchi S, Nagano T, Matsuki N, Ikegaya Y (2014) Unbalanced excitability underlies offline reactivation of behaviorally activated neurons. Nat Neurosci 17:503–505
23. Muller D, Buchs PA, Stoppini L (1993) Time course of synaptic development in hippocampal organotypic cultures. Brain Res Dev Brain Res 71:93–100
24. Namiki S, Norimoto H, Kobayashi C, Nakatani K, Matsuki N, Ikegaya Y (2013) Layer III neurons control synchronized waves in the immature cerebral cortex. J Neurosci 33:987–1001
25. Pare D, Shink E, Gaudreau H, Destexhe A, Lang EJ (1998) Impact of spontaneous synaptic activity on the resting properties of cat neocortical pyramidal neurons In vivo. J Neurophysiol 79:1450–1460
26. Pavlides C, Winson J (1989) Influences of hippocampal place cell firing in the awake state on the activity of these cells during subsequent sleep episodes. J Neurosci 9:2907–2918
27. Penn AA, Shatz CJ (1999) Brain waves and brain wiring: the role of endogenous and sensory-driven neural activity in development. Pediatr Res 45:447–458
28. Petersen CC, Hahn TT, Mehta M, Grinvald A, Sakmann B (2003) Interaction of sensory responses with spontaneous depolarization in layer 2/3 barrel cortex. Proc Natl Acad Sci USA 100:13638–13643
29. Raichle ME (2006) Neuroscience. The brain's dark energy. Science 314:1249–1250
30. Ranck JB Jr (1973) Studies on single neurons in dorsal hippocampal formation and septum in unrestrained rats. I. Behavioral correlates and firing repertoires. Exp Neurol 41:461–531
31. Redman SJ, Lampard DG, Annal P (1968) Monosynaptic stochastic stimulation of cat spinal motoneurons. II. Frequency transfer characteristics of tonically discharging motoneurons. J Neurophysiol 31:499–508
32. Rochefort NL, Garaschuk O, Milos RI, Narushima M, Marandi N, Pichler B, Kovalchuk Y, Konnerth A (2009) Sparsification of neuronal activity in the visual cortex at eye-opening. Proc Natl Acad Sci USA 106:15049–15054
33. Sanchez-Vives MV, McCormick DA (2000) Cellular and network mechanisms of rhythmic recurrent activity in neocortex. Nat Neurosci 3:1027–1034
34. Sasaki T, Matsuki N, Ikegaya Y (2007) Metastability of active CA3 networks. J Neurosci 27:517–528
35. Sasaki T, Takahashi N, Matsuki N, Ikegaya Y (2008) Fast and accurate detection of action potentials from somatic calcium fluctuations. J Neurophysiol 100:1668–1676
36. Shu Y, Hasenstaub A, Badoual M, Bal T, McCormick DA (2003) Barrages of synaptic activity control the gain and sensitivity of cortical neurons. J Neurosci 23:10388–10401
37. Softky WR (1995) Simple codes versus efficient codes. Curr Opin Neurobiol 5:239–247
38. Stepanyants A, Martinez LM, Ferecsko AS, Kisvarday ZF (2009) The fractions of short- and long-range connections in the visual cortex. Proc Natl Acad Sci U S A 106:3555–3560
39. Stoppini L, Buchs PA, Muller D (1991) A simple method for organotypic cultures of nervous tissue. J Neurosci Methods 37:173–182
40. Stuart G, Schiller J, Sakmann B (1997) Action potential initiation and propagation in rat neocortical pyramidal neurons. J Physiol 505(Pt 3):617–632
41. Takahashi N, Sasaki T, Usami A, Matsuki N, Ikegaya Y (2007) Watching neuronal circuit dynamics through functional multineuron calcium imaging (fMCI). Neurosci Res 58:219–225
42. Takahashi N, Sasaki T, Matsumoto W, Matsuki N, Ikegaya Y (2010) Circuit topology for synchronizing neurons in spontaneously active networks. Proc Natl Acad Sci U S A 107:10244–10249
43. Takahashi N, Kitamura K, Matsuo N, Mayford M, Kano M, Matsuki N, Ikegaya Y (2012) Locally synchronized synaptic inputs. Science 335:353–356
44. Traynelis SF (1998) Software-based correction of single compartment series resistance errors. J Neurosci Methods 86:25–34

45. Wang J, Zhao P, Hoi SCH (2012) Exact soft confidence-weighted learning. Int Conf Mach Learn Proc 1206:4612
46. Yamamoto N, Kurotani T, Toyama K (1989) Neural connections between the lateral geniculate nucleus and visual cortex in vitro. Science 245:192–194
47. Zhang LI, Poo MM (2001) Electrical activity and development of neural circuits. Nat Neurosci 4:1207–1214

OPEN ACCESS Freely available online

PLOS ONE

Dopamine Receptor Activation Reorganizes Neuronal Ensembles during Hippocampal Sharp Waves *In Vitro*

Takeyuki Miyawaki[1], Hiroaki Norimoto[1], Tomoe Ishikawa[1], Yusuke Watanabe[1], Norio Matsuki[1], Yuji Ikegaya[1,2]*

1 Laboratory of Chemical Pharmacology, Graduate School of Pharmaceutical Sciences, The University of Tokyo, Bunkyo-ku, Tokyo, Japan, **2** Centre for Information and Neural Networks, Suita City, Osaka, Japan

Abstract

Hippocampal sharp wave (SW)/ripple complexes are thought to contribute to memory consolidation. Previous studies suggest that behavioral rewards facilitate SW occurrence *in vivo*. However, little is known about the precise mechanism underlying this enhancement. Here, we examined the effect of dopaminergic neuromodulation on spontaneously occurring SWs in acute hippocampal slices. Local field potentials were recorded from the CA1 region. A brief (1 min) treatment with dopamine led to a persistent increase in the event frequency and the magnitude of SWs. This effect lasted at least for our recording period of 45 min and did not occur in the presence of a dopamine D_1/D_5 receptor antagonist. Functional multineuron calcium imaging revealed that dopamine-induced SW augmentation was associated with an enriched repertoire of the firing patterns in SW events, whereas the overall tendency of individual neurons to participate in SWs and the mean number of cells participating in a single SW were maintained. Therefore, dopaminergic activation is likely to reorganize cell assemblies during SWs.

Citation: Miyawaki T, Norimoto H, Ishikawa T, Watanabe Y, Matsuki N, et al. (2014) Dopamine Receptor Activation Reorganizes Neuronal Ensembles during Hippocampal Sharp Waves *In Vitro*. PLoS ONE 9(8): e104438. doi:10.1371/journal.pone.0104438

Editor: Liset Menendez de la Prida, Consejo Superior de Investigaciones Cientificas - Instituto Cajal, Spain

Received January 15, 2014; **Accepted** July 14, 2014; **Published** August 4, 2014

Funding: This work was supported by Grants-in-Aid for Science Research on Innovative Areas (22115003; 25119004) (http://www.jsps.go.jp/english/e-grants/grants01.html) and the Japan Society for the Promotion of Science through the Funding Program for Next Generation World-Leading Researchers (NEXT Program), initiated by the Council for Science and Technology Policy (LS023) (http://www.jsps.go.jp/english/e-jisedai/index.html). The funders had no role in study design, data collection and analysis, decision to publish, or preparation of the manuscript.

Competing Interests: The authors have declared that no competing interests exist.

* Email: ikegaya@mol.f.u-tokyo.ac.jp

Introduction

Hippocampal sharp wave (SW)/ripples are a complex of relatively slow (10–30 Hz) field transients and fast (150–250 Hz) field oscillations and are observed in the hippocampus during slow wave sleep and quiet awake states [1–3]. SW/ripples represent transient neuronal synchronization that originates mainly from the CA3 region and propagates to CA1 and the downstream networks [4]. A current hypothesis on learning and memory implies that labile hippocampal memory traces are transferred to a more stable neocortical storage [5] through offline reverberatory replays of behavioral experiences during SW/ripples [6]. In support of this concept, selective suppression of SWs results in an impairment of long-term memory formation [7].

SW/ripples are reported to increase when a rat is rewarded or placed in a novel environment [8,9]. Because both situations increase dopaminergic neuronal activities [10,11], dopamine is one of the candidate neuromodulators of the SWs/ripple facilitation, although other modulators such as opioids [12] and orexin [13] are also released during rewarding. Dopaminergic neurons project to various regions in the brain [14], and it remains to be elucidated whether this enhancement is caused directly by dopamine receptor activation in the hippocampus or indirectly by other neural pathways. We hypothesize that hippocampal dopamine directly increases SW/ripple occurrence, based on the following three reasons. First, the ventral tegmental area, a brain reward system, projects its dopaminergic axons to the hippocampus [15]. Second, the extracellular concentration of dopamine in the hippocampus rises in response to novel environmental stimuli [16]. Finally, bilateral injection of a D_1/D_5 receptor agonist into the hippocampus enhances memory retention [17], whereas a D_1/D_5 receptor antagonist disturbs one-day memory without affecting shorter-term memory [18].

An *in vitro* model of SW/ripples in acute hippocampal slices is usable to examine the effects on pharmacological reagents [19–26]. Moreover, the *in vitro* approach using functional multineuron calcium imaging (fMCI) enable us to reveal the spatiotemporal cellular patterns of SW/ripple activity [23,27]. fMCI is a large-scale optical recording technique that records action potentials *en masse* from a neuron population, by taking advantage of the fact that an action potential reliably evokes a transient increase in the calcium ion concentration of the cell body of the monitored neuron. We exploited this *in vitro* assay system and investigated how dopamine modulates the occurrence of SWs and their internal structures. Our data showed that transient dopamine receptor activation induced a persistent increase in SW occurrence via dopamine D_1/D_5 receptors. This facilitation was accompanied by a reorganization of spiking patterns in SWs.

Results

Local field potentials (LFPs) were recorded from CA1 stratum pyramidale of hippocampal slices that were obliquely cut at an angle of 12.7° in the fronto-occipital direction (Fig. 1A and 1B).

Slices that were perfused with artificial cerebrospinal fluid (aCSF) at 7–9 ml/min for > 1.5 h spontaneously exhibited SWs, as reported previously [23]. The SW events occurred together with ripple oscillations (Fig. 1C). The mean frequency of SW events was 0.42±0.17 Hz (mean ± SD of 55 slices) and did not differ from that reported in *in vivo* studies [28].

To examine the effect of dopamine receptor activation on SWs, we perfused hippocampal slices with 1 μM dopamine for 1 min. Immediately after dopamine washout, SW events started to increase gradually in frequency. Within 10–20 min, the effect reached a steady state at 160.0±17.2% relative to the baseline level and persisted at least for our observation period of 45 min (Fig. 2A–C, mean ± SEM of 9 slices, $P = 0.0082$, $t_8 = 3.49$, paired *t*-test *versus* the baseline period). The bath application of dopamine also increased the peak amplitude of the LFP deflections during SWs to 120.6±8.7% (Fig. 2D, $P = 0.045$, $t_8 = 2.37$, paired *t*-test). This result suggests that after the dopamine challenge, CA1 networks received stronger synaptic inputs from CA3 networks during SWs. On the other hand, the mean power of ripple oscillations, which were measured between 150 Hz and 250 Hz in the fast Fourier transform of LFP traces, did not significantly change (Fig. 2E, $P = 0.069$, $t_8 = 1.65$, paired *t*-test), suggesting that dopamine exerted little effect on the population firing level of CA1 neurons; however note that the tendency of the ripple power change was in the same direction as the SW amplitude change and could become significant if the number of data was increased.

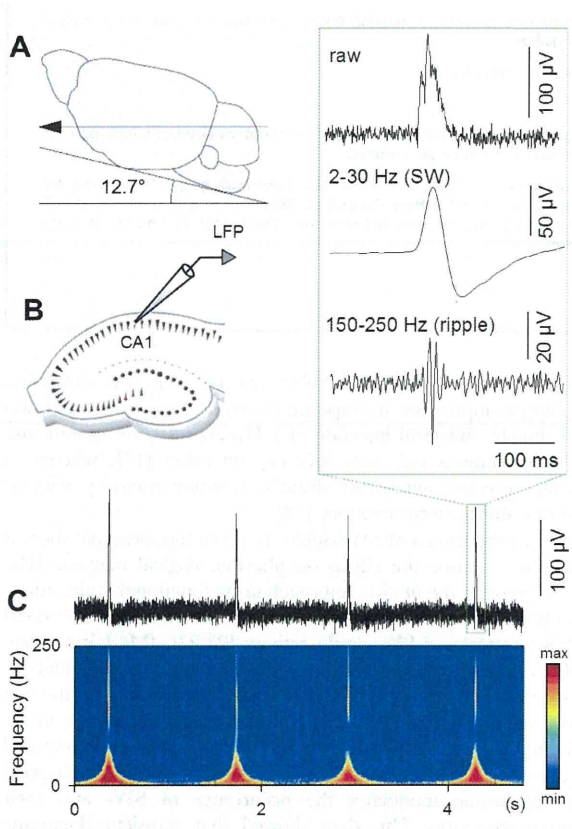

Figure 1. SW/ripples occur spontaneously in obliquely sliced hippocampal preparations. A. The brains of 3-to-4-week-old mice were sliced at an angle of 12.7° in the fronto-occipital direction. **B.** LFPs were recorded from CA1 stratum pyramidale of the hippocampal slices. **C.** An example of LFP recording. The top raw trace was wavelet-analyzed into the bottom power spectrogram. The inset indicates magnifications of raw (top), 2–30-Hz-filtered (middle, SW), and 150–250-Hz-filtered (bottom, ripple) traces.
doi:10.1371/journal.pone.0104438.g001

To examine the subtypes of dopamine receptors involved in this phenomenon, we applied dopamine in aCSF containing either 0.1 μM SCH23390, a dopamine D_1/D_5 receptor antagonist, or 1 μM sulpiride, a dopamine D_2 receptor antagonist. Either antagonist alone did not affect SW frequency or amplitude during the baseline period before dopamine application (Fig. 3A–C; frequency: sulpiride, $P = 0.45$, $t_3 = 0.86$, SCH23390, $P = 0.74$, $t_5 = 0.35$; amplitude: sulpiride, $P = 0.97$, $t_3 = 0.045$, SCH23390, $P = 0.96$, $t_5 = 0.057$, paired *t*-test). In the presence of SCH23390, dopamine did not increase the frequency or amplitude of SWs (Fig. 3D and 3E, 92.1±18.7%, $P = 0.69$, $t_5 = 0.42$; Fig. 3F, 109.4±30.7%, $P = 0.77$, $t_5 = 0.31$; paired *t*-test), whereas it did in the presence of sulpiride (Fig. 3D and 3E, 143.1±15.5%, $P = 0.032$, $t_6 = 2.78$, paired *t*-test). The same tendency was observed in their amplitudes (Fig. 3F, 117.8±7.56%, $P = 0.035$, $t_6 = 2.71$, paired *t*-test). Thus, D_1/D_5 receptors are likely to mediate dopamine-induced SW facilitation. To further confirm this, we applied 30 μM SKF38393, a D_1/D_5 receptor agonist, for 1 min. SKF38393 induced a long-lasting facilitation of the SW event frequency (Fig. 3G and 3H, 149.6±14.6%, $P = 0.0017$, $t_{12} = 4.02$, paired *t*-test). This facilitation exhibited a time course similar to the effect of dopamine (Fig. 2) and was also accompanied by an increase in the SW amplitude (Fig. 3I, 142.0±17.3%, $P = 0.017$, $t_{12} = 2.78$, paired *t*-test). The effect of SKF38393 was not observed in the presence of 0.1 μM SCH23390 (Fig. 3H and 3I, $P = 0.96$, $t_4 = 0.055$; Fig. 3I, $P = 0.47$, $t_4 = 0.79$, paired *t*-test). In the following experiments, therefore, we used SKF38393, but not dopamine, to stimulate D1/D5 receptors specifically.

Tetanic stimulation to Schaffer collaterals is known to induce long-term potentiation (LTP) at CA3-CA1 synapses and CA3 recurrent synapses, and also to increase the incidence of SW/ripples [21], which suggests that synaptic strengthening can facilitate SW occurrence. In addition, D_1/D_5 receptor activation is known to induce LTP-like facilitation at CA3-CA1 synapses, although the effect appears slowly [29]. In our experimental system, we confirmed that 1-min treatment with 30 μM SKF38393 did not induce LTP at CA3-CA1 synapses within 45 min during which period SWs were already facilitated (Fig. 3J; amplitude, $P = 0.56$, $t_2 = 0.69$; slope, $P = 0.66$, $t_2 = 0.52$, paired *t*-test). Thus, LTP is unlikely to account for the SW facilitation observed in this study.

During SW/ripples, specific subsets of neurons fire action potentials [21,24,30–33], exhibiting a rich repertoire of the internal patterns of SWs (*i.e.*, various combinations of activated neurons) [24,34,35]; however, LFP recordings alone cannot determine whether the dopamine-increased occurrence of SWs reflected an increase in the repetitions of the same SW patterns or an increase in the SW pattern variability. To address this question, we used fMCI, an optical technique that records spikes through action potential-evoked calcium elevations in the cell bodies of the focused neurons [36], because unit activities were not evident in our LFP recordings. A drawback of the fMCI technique is its low time resolution due to slow calcium signal kinetics, so that we could not resolve individual spikes during a SW/ripple event. In the present study, therefore, we focused on the combinations (patterns) of neurons that participated in individual SW events, rather than the temporal spike sequences during the SWs.

Oregon Green BAPTA1 AM (OGB1) was bolus-injected into CA1 stratum pyramidale (Fig. 4A), and the fluorescence of OGB1 was monitored at 50 frames per second from CA1 cells in an area of approximately 400×250 μm^2, which contained an average of

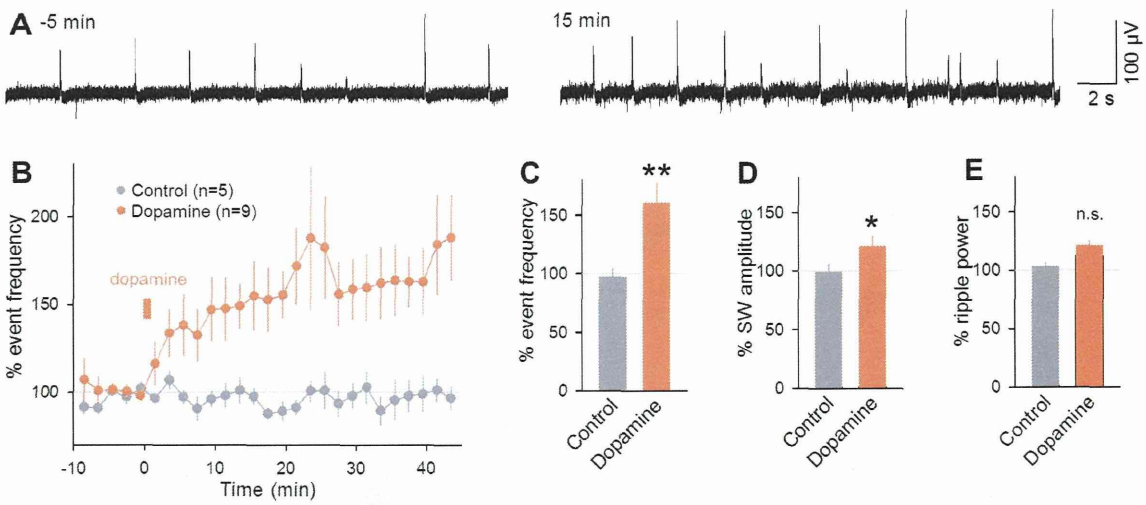

Figure 2. Bath application of dopamine induces long-lasting facilitation of SW events. A. Representative traces of CA1 LFPs recorded 5 min before (left) and 15 min after (right) 1-min application of 1 μM dopamine. **B.** Time course of the percentage of the frequency of SW events relative to the mean value during a 6-min period prior to the dopamine application. Slices were bath-perfused with 1 μM dopamine for 1 min at time 0–1 min. Control slices were perfused continuously with normal extracellular solution. **C–E.** The mean ratios of the SW event frequency (C), the SW amplitude (D), and the ripple power (150–250 Hz) (E) were calculated from the −5-to-0 min period and the 30-to-35 min period. $^{**}P = 0.0082$, $t_8 = 3.49$; $^{*}P = 0.045$, $t_8 = 2.37$, paired *t*-test *versus* the −5-to-0 min period. Data are the means ± SEMs of 9 and 5 slices from 7 and 3 mice.
doi:10.1371/journal.pone.0104438.g002

45.8±15.4 OGB1-loaded neurons (mean ± SD of 8 slices). Neurons spontaneously exhibited transient $\Delta F/F$ rises in their cell bodies (Fig. 4B). The calcium transients were associated with spikes of the neurons, and even single spikes were detectable in $\Delta F/F$ traces (Fig. 4C). LFPs were simultaneously recorded from CA1 stratum pyramidale in the same microscopic field (Fig. 4A and 4B).

We plotted a peri-SW time histogram for the timings of calcium events relative to the SW peak time (Fig. 4D, $n = 7{,}709$ calcium events in 252 cells from 8 slices). The histogram exhibited an evident peak at time 0 ms. The mean firing rates started to increase at approximately −200 ms and suddenly dropped to nearly zero at 50 ms. Therefore, we defined SW-locked activities as calcium events that occurred within a time window between −200 ms and 50 ms relative to the SW peak time. Not all calcium events were time-locked to SWs; 252 neurons (68.9%) of a total of 366 neurons in 8 slices exhibited at least one calcium activity during our imaging period of 3 min. Among these active neurons, 199 neurons (79.0%) were SW participants; they exhibited at least one SW-locked activity. Of a total of 7,709 calcium transients emitted by all 252 active cells, 3,597 (46%) were SW-locked activities. On average, a single SW event recruited 4.0±5.6% of the total OGB1-loaded 366 neurons (mean ± SD of =1,871 SWs). A single SW-participating neuron participated in 4.8±4.9% SW events (mean ± SD, $n = 199$ neurons).

To examine how these patterned SW activities are modified by D_1/D_5 dopamine receptor activation, we bath-applied 30 μM SKF38393 for 1 min. The imaging period was limited to a total of 6 min to minimize laser illumination-induced photobleaching and phototoxicity. We compared the activity patterns between two 3-min periods immediately before and about 20 min after application of SKF38393 (Fig. 4E). For each period, we analyzed 795 and 1,076 SW events, which involved 3,714 and 3,995 calcium transients, respectively. To quantify the effect of D_1/D_5 receptor activation on the distribution of SW-associated firing (Fig. 4D), we calculated the mean time lag from the SW peaks (Fig. 4F) and the skewness (Fig. 4G) and kurtosis (Fig. 4H) of the peri-SW time histogram of calcium transients. None of these parameters differed significantly between the periods before and after SKF38393 application, suggesting that D_1/D_5 receptor activation does not change the SW-locked firing properties (mean, $P = 0.35$, $t_7 = 1.01$; skewness, $P = 0.12$, $t_7 = 1.77$; kurtosis, $P = 0.48$, $t_7 = 0.75$, paired *t*-test).

We also analyzed the spike rates during SWs and during the remaining periods between SWs. The mean rates of calcium transients during SWs were 1.5±2.1 and 1.6±1.9 activities/min/cell before and after SKF38393 application, respectively (mean ± SD of 366 cells, $P = 0.55$, $t_7 = 0.62$, paired *t*-test), whereas the mean activity rates during SW-free periods were 1.7±1.2 and 1.9±2.0 activities/min/cell before and after SKF38393 application ($P = 0.66$, $t_7 = 0.46$, paired *t*-test). We also compared the level of spike synchronization between a pair of neurons. We defined $N_{1\&2}/(N_1+N_2-N_{1\&2})$ as a synchrony index, where N_1 and N_2 denote the total numbers of calcium transients in neuron #1 and neuron #2, respectively, and $N_{1\&2}$ denotes the total number of calcium transients emitted jointly by these neurons in a time window of 250 ms. The synchrony index did not correlate between the 'in-SW' and the 'inter-SW' periods (Fig. 4I left; $R^2 = 0.004$), suggesting that SWs actively recruit different cell assemblies from neuron populations synchronizing during SW-free periods. This tendency was maintained after SKF38393 application (Fig. 4I right; $R^2 = 0.016$).

Next, we examined the population dynamics. During the baseline period, 38.5% neurons were SW participants (Fig. 5A right, $n = 141$ cells). This ratio slightly increased to 43.9% ($n = 161$ cells) after SKF38393 application, but this change was not statistically significant ($n = 366$ cells; $P = 0.41$, $Z = 1.48$, *Z*-test for the equality of two proportions). The SW participants before and after SKF38393 application shared 28.1% common neurons. This overlap ratio was significantly higher than the stochastically expected ratio of 16.9% ($P = 1.62\times10^{-8}$, $Z = 5.65$, *Z*-test for a proportion), suggesting that dopamine receptor activation did not

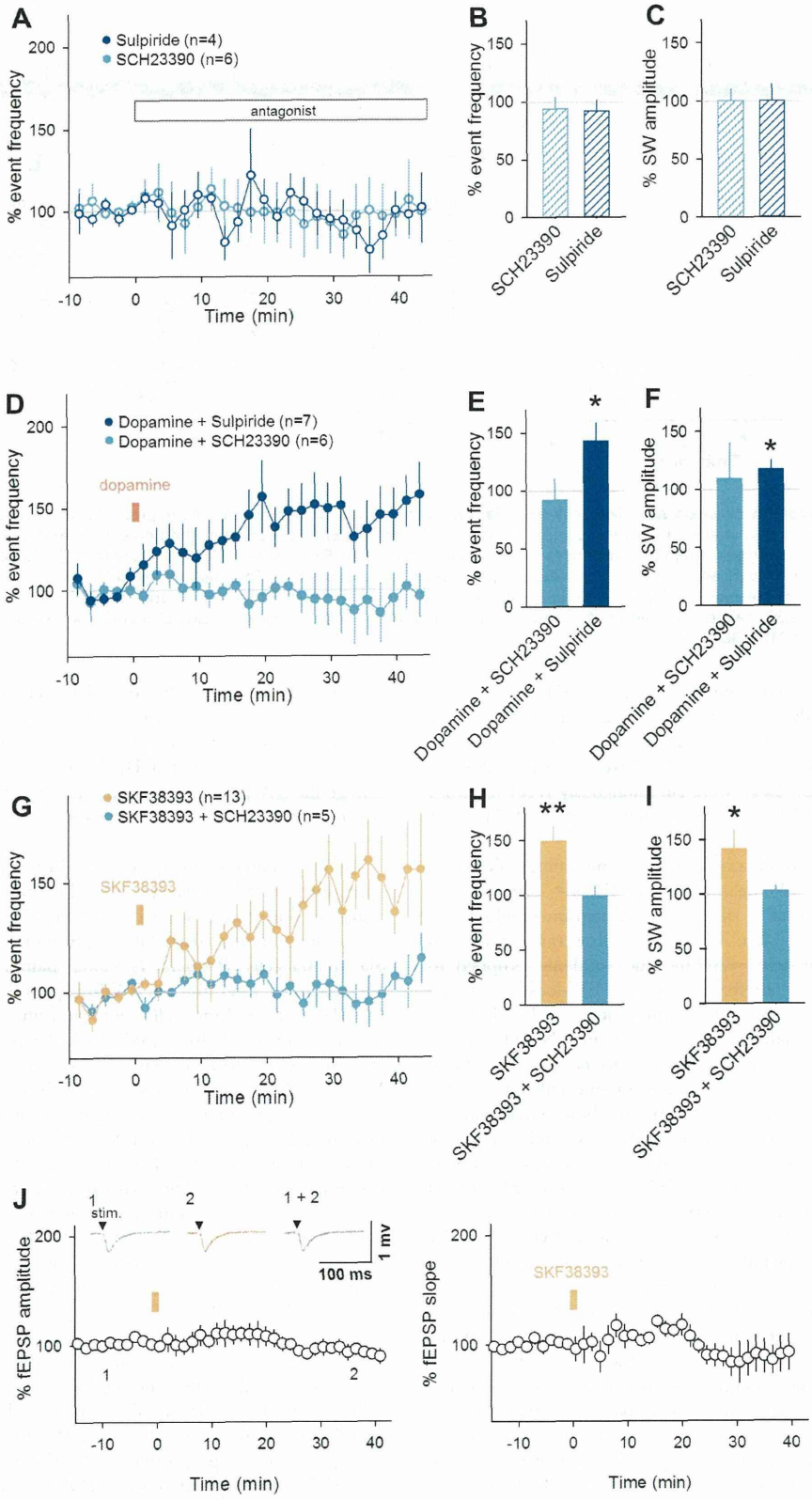
A
Sulpiride (n=4)
SCH23390 (n=6)
antagonist
% event frequency
Time (min)
B
% event frequency
SCH23390
Sulpiride
C
% SW amplitude
SCH23390
Sulpiride
D
Dopamine + Sulpiride (n=7)
Dopamine + SCH23390 (n=6)
dopamine
% event frequency
Time (min)
E
% event frequency
Dopamine + SCH23390
Dopamine + Sulpiride
F
% SW amplitude
Dopamine + SCH23390
Dopamine + Sulpiride
G
SKF38393 (n=13)
SKF38393 + SCH23390 (n=5)
SKF38393
% event frequency
Time (min)
H
% event frequency
SKF38393
SKF38393 + SCH23390
I
% SW amplitude
SKF38393
SKF38393 + SCH23390
J
1 stim.
2
1 + 2
1 mv
100 ms
% fEPSP amplitude
Time (min)
SKF38393
% fEPSP slope
Time (min)

Figure 3. D_1/D_5 receptor activation is responsible for dopamine induced SW facilitation. A. Time course of the percentage of the frequency of SW events relative to the mean value during the pre-application period while the slices were perfused with 0.1 μM SCH23390, a D_1/D_5 receptor antagonist, and 1 μM sulpiride, a D_2 receptor antagonist, from time 0–45 min. **B–C.** The mean SW event frequency (B) and the mean SW amplitude (C) at time 30–35 min. **D.** Slices were perfused with 1 μM dopamine for 1 min at time 0 in the continuous presence of 0.1 μM SCH23390 or 1 μM sulpiride. **E–F.** The mean SW event frequency (E) and the mean SW amplitude (F) at time 30–35 min. $^*P = 0.032$, $t_6 = 2.78$, $^*P = 0.035$, $t_6 = 2.71$, paired *t*-test *versus* the −5-to-0 min period. Data are the means ± SEMs of 7 and 6 slices from 4 and 3 mice, respectively. **G.** Slices were perfused with 30 μM SKF38393 at time 0 in the absence (orange) and the continuous presence (light blue) of 0.1 μM SCH23390, a D_1/D_5 receptor antagonist. **H–I.** The mean SW event frequency (H) and the mean SW amplitude (I) at time 30–35 min. $^{**}P = 0.0017$, $t_{12} = 4.02$ (H); $^*P = 0.017$, $t_{12} = 2.78$ (I), paired *t*-test *versus* the −5-to-0 min period. Data are the means ± SEMs of 13 and 5 slices from 10 and 3 mice, respectively. **J.** While fEPSPs evoked by field stimulation of Schaffer collaterals were recorded from CA1 stratum radiatum, slices were perfused with 30 μM SKF38393 for 1 min at time 0. Time changes in fEPSP amplitudes (left) and slopes (right) are plotted as mean ± SEMs of 3 slices from 3 mice. The insets indicate example traces at two time points.

doi:10.1371/journal.pone.0104438.g003

actively change SW-participating cell populations. To confirm this idea, we have examined how activity of neuronal populations drift spontaneously under the control conditions without drug application [37]. We continuously perfused aCSF without SKF38393 (control aCSF) and compared the activity patterns between two 3-min periods intervened by 20 min, which corresponded to the time course of the experiments with SKF38393 application. For the two periods, we analyzed 377 and 405 SW events, which involved 1,465 and 1,321 calcium transients, respectively ($n = 253$ cells in 5 slices from 5 mice). SW participants were 45.4% (115 cells) in the first 3-min period and 46.6% (118 cells) in the second 3-min period, and 32.4% (82 cells) participated in both periods (Fig. 5A left). The overlap ratio was again significantly higher than the chance ratio of 21.2% ($P = 1.85\times10^{-5}$, $Z = 4.28$, *Z*-test for a proportion). Importantly, the overlap ratios did not differ between control and SKF38393 experiments ($P = 0.30$, $Z = 1.15$, *Z*-test for the equality of two proportion), supporting our idea that SKF38393 did not actively change SW-participating cell populations.

At a more microscopic level, the SW-locked activity frequencies of individual neurons were positively correlated before and after SKF38393 application (Fig. 5B right, $R^2 = 0.64$, $P = 3.7\times10^{-83}$, $t_{364} = 25.5$, *t*-test for a correlation coefficient). A similar tendency was observed in control slices without SKF38393 application (Fig. 5B left, $R^2 = 0.57$, $P = 5.0\times10^{-48}$, $t_{251} = 18.3$), and the correlation coefficients did not differ between control and SKF38393 experiments ($P = 0.57$, $Z = 0.57$, *Z*-test for two correlation coefficients). Thus, dopamine receptor activation did not alter the tendency of SW participation of individual neurons. Moreover, dopamine receptor activation did not change the mean number of neurons participating in single SW events (Fig. 5C right; $P = 0.25$, $t_7 = 1.23$, paired *t*-test), as did in the control group (Fig. 5C left, $P = 0.93$, $t_4 = 0.098$, paired *t*-test). The mean amplitudes of calcium transients in each cell were little correlated before and after SKF38393 application, as were in the control group (Fig. 5D, control: $R^2 = 0.091$, SKF38393, $R^2 = 0.00025$, $P = 0.13$, $Z = 1.53$, *Z*-test for two correlation coefficients).

We sought to examine whether the effect of D_1/D_5 receptor activation was different between excitatory and inhibitory neurons. In our imaging experiments, the neuron types were not separable by the OGB1 appearance or the firing rates [38], but it is known that interneurons constitute 20% of the total CA1 cells [39] and that interneurons are more tightly time-locked to SW events compared to excitatory neurons [40]. Therefore, we expediently regarded the top 20% cells for the 'SW-locked' probability, the ratio of SW-locked activities to the total SW events, during the baseline period as putative interneurons and the others as putative pyramidal neurons. For both groups, we compared the mean SW-locked probability, the mean amplitude of calcium transients, and the population of SW-participating cells before and after SKF38393 application (Fig. 6). For the SW-locked probability, either groups did not show statistically significant changes (top 20%, Fig. 6A left; $P = 0.11$, $t_7 = 1.82$, paired *t*-test, bottom 80%, Fig. 6A right; $P = 0.23$, $t_7 = 1.32$, paired *t*-test). However, SKF38393 significantly increased the amplitudes of SW-locked calcium transients of putative pyramidal neurons, but not in putative interneurons (top 20%, Fig. 6B left; $P = 0.09$, $t_7 = 1.98$, paired *t*-test, bottom 80%, Fig. 6B right; $P = 0.016$, $t_7 = 3.14$, paired *t*-test). Putative interneurons did not exhibit a cell population shift after SKF38393 application, and the populations of SW participants were more overlapped before and after SKF38393 application, compare to those in control slices (Fig. 6C; $P<10^{-20}$, $Z = 12.0$, *Z*-test for the equality of two proportion). Therefore, D_1/D_5 receptor activation seemed to exert a more effect on pyramidal neurons than on interneurons.

We then focused on the internal patterns of SW events. First, we extracted SW-locked activities and generated a SW-activity matrix in which SW-locked activities were arranged in a space of the cell number (row) *versus* the SW event number (column) (Fig. 7A). We binarized this matrix so that the matrix elements with SW events were '1' (activated), whereas the others were '0' (not-activated). To evaluate the pattern similarity between two given SWs, we calculated the correlation coefficient between two binary vectors of the corresponding SW events. We repeated this calculation for all possible SW pairs in the SW-activity matrix and created a correlation matrix (Fig. 7B). As a whole, the correlation coefficients were lower after SKF38393 application compared to those observed before the application (Fig. 7C right; $P = 2.7\times10^{-15}$, $D = 0.184$, Kolmogorov-Smirnov test), whereas the distribution of the correlation coefficients did not shift in the control group (Fig. 7C left). Thus, SWs became more dissimilar to one another after dopamine D_1/D_5 receptor activation. We thus hypothesized that SKF38393 increases a repertoire of SW patterns. To examine this possibility, we applied the affinity propagation algorithm, an iterative clustering method [41], to the correlation matrix. Based on the SW pattern similarity, this algorithm unsupervisedly determined the total number of SW subgroups (clusters) that existed in the matrices (Fig. 7D) [42]. We found that the number of SW clusters increased after SKF38393 application (Fig. 7E right; $P = 0.030$, $t_7 = 2.25$, paired *t*-test, $n = 8$ slices), but not after no drug application (Fig. 7E left; $P = 0.78$, $t_4 = 0.30$, paired *t*-test, $n = 5$ slices). We repeated the same analysis for a time window between −50 and +50 ms relative to the SW peak, which period is more often used in previous literature about SWs. We obtained the same result (Fig. 7F; control: $P = 0.54$, $t_4 = 0.68$, paired *t*-test, $n = 5$ slices; SKF38393: $P = 0.036$, $t_7 = 2.12$, paired *t*-test, $n = 8$ slices). Thus, we conclude that dopamine D_1/D_5 receptor activation led to the emergence of different patterns of SWs. To exclude the possibility that the increased SW patterns were merely due to an increase in the statistical chance of cell combinations, which could came from a slight increase in the number of SW-participating neurons (see Fig. 5A right), we examined the

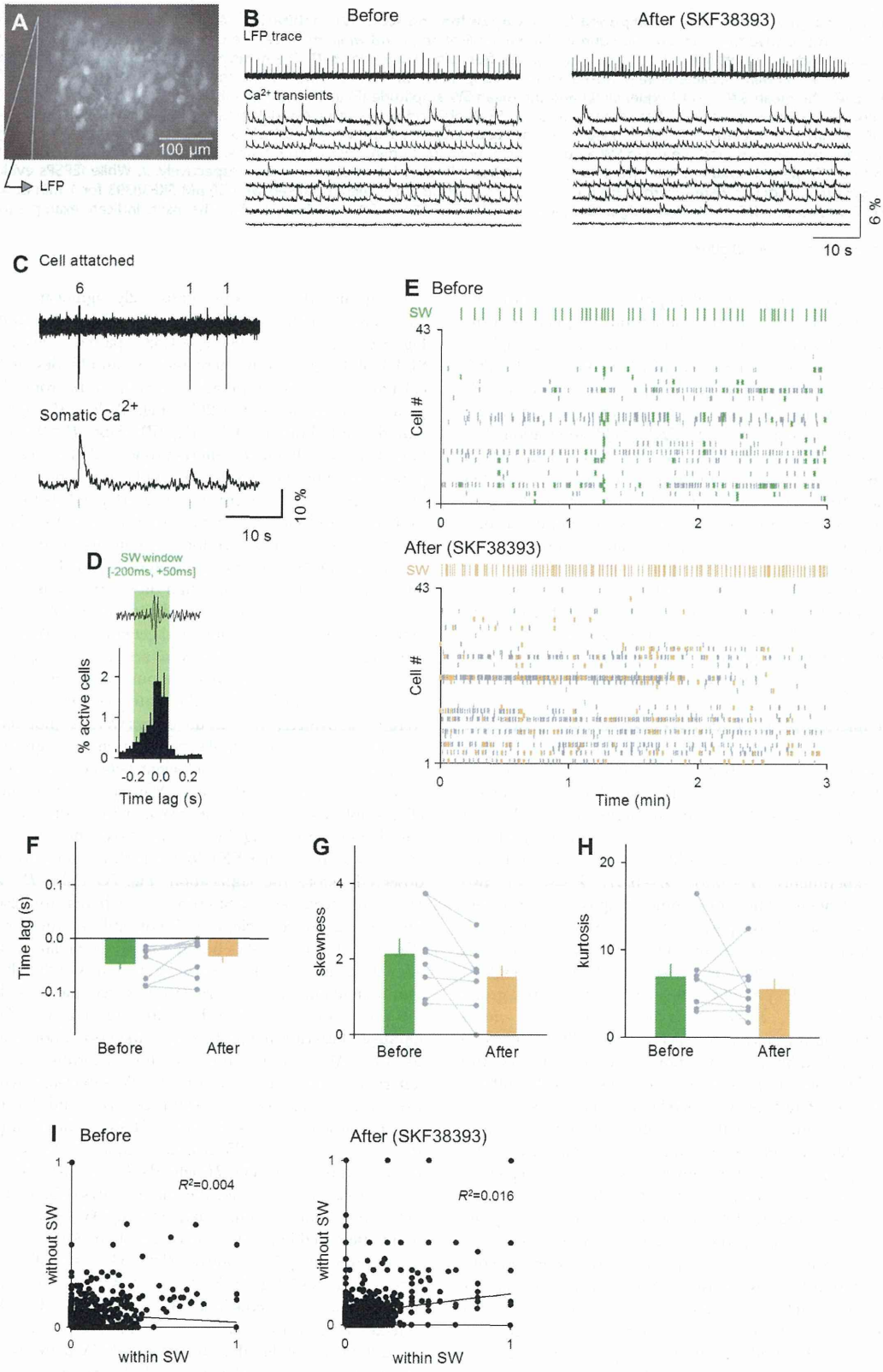
A
100 µm
LFP
B
Before
LFP trace
Ca2+ transients
After (SKF38393)
6 %
10 s
C
Cell attatched
6
1
1
Somatic Ca2+
10 %
10 s
D
SW window
[-200ms, +50ms]
% active cells
Time lag (s)
E
Before
SW
Cell #
After (SKF38393)
Time (min)
F
Time lag (s)
Before
After
G
skewness
H
kurtosis
I
Before
R2=0.004
without SW
within SW
After (SKF38393)
R2=0.016